ELSEVIER

Journal of Nuclear Materials 297 (2001) 313–326

journal of nuclear materials

www.elsevier.com/locate/jnucmat

Factors governing microstructure development of Cr_2O_3-doped UO_2 during sintering

L. Bourgeois [a], Ph. Dehaudt [a,*], C. Lemaignan [a], A. Hammou [b]

[a] *Commissariat à l'Energie Atomique/Département d'Etude des Combustibles, CEA Grenoble, 17 Rue des Martyrs, 38054 Grenoble cedex 9, France*

[b] *Université Joseph Fourier de Grenoble France*

Received 4 April 2001; accepted 21 May 2001

Abstract

Sintering and grain growth of compacted uranium dioxide powder pellets doped with Cr_2O_3 were investigated at constant heating rates ranging from 75 to 500 K h^{-1}. The influence of parameters such as the oxygen potential of the sintering atmosphere and pellet green density on the final microstructure was studied. Dilatometric analysis and monitoring of microstructural development revealed a phenomenon of abnormal grain growth promoting densification. The existence of a eutectic between Cr and Cr_2O_3 is also discussed. Grain growth does not appear to be widely affected by small differences in residual porosity, which is a function of green density, so that it is possible to propose a solubility limit for Cr_2O_3 in stoichiometric UO_2 at 1700°C. Examination of microstructural changes during annealing, with or without pore formers, showed the existence of limiting grain sizes for doped samples above the solubility limit. Lastly, experimental sintering conditions need to be checked in order to obtain reproducible results.

Résumé

Le frittage et la croissance cristalline de poudres d'UO_2 compactées et dopées avec du Cr_2O_3 ont été examinés pour des vitesses de chauffage allant de 75 à 500 K h^{-1}. L'influence de paramètres comme le potentiel d'oxygène des atmosphères de frittage et la densité en cru des pastilles sur la microstructure finale a été étudiée. Par analyse dilatométrique et suivi de l'évolution microstructurale, un stade de croissance cristalline anormale favorisant la densification a été mis en évidence. L'existence d'un eutectique entre Cr et Cr_2O_3 est également discutée. La croissance cristalline est peu affectée par le volume poreux résiduel, fonction de la densité des crus, ce qui a permis de proposer une limite de solubilité pour Cr_2O_3 dans l'UO_2 stoechiométrique à 1700°C. Le suivi de l'évolution des microstructures lors des recuits, en présence ou non de porogène, a fait apparaître des tailles de grains maximales pour les échantillons dopés au-dessus de la limite de solubilité. Enfin, un contrôle des conditions expérimentales de frittage est nécessaire afin d'obtenir des résultats reproductibles.

1. Introduction

Obtaining reproducible microstructures in terms of both particle size and relative density is of crucial importance for nuclear ceramics. After sintering and heating for a few hours at about 1700°C in reducing atmospheres, the particle size of pure UO_2 is about 10 μm. The reasons for modifying this size significantly (by about an order of magnitude) have been discussed elsewhere, together with the classical methods for doing so [1,2]. The consequences of adding minimal amounts of Cr_2O_3 on the densification and grain growth of uranium dioxide will be examined here.

The activation of UO_2 grain growth by adding Cr_2O_3 was illustrated by Ainscough et al. [3] and Killeen [4], and this doped fuel was irradiated in both cases.

* Corresponding author.
E-mail address: dehaudt@cea.fr (P. Dehaudt).

0022-3115/01/$ - see front matter
PII: S0022-3115(01)00626-2

Ainscough et al. [3] claim to have obtained grains of about 80 μm with an addition of 0.3 wt% and Killeen claims 50 μm with of 0.5 wt% of Cr_2O_3 instead of 6 μm for the test specimens. These works do not discuss the methods used in preparing the mixes, nor the heating cycles adopted, nor the oxygen potential of the sintering atmosphere used. Moreover, the results obtained by Killeen [4] do not specify whether a fraction of the chromium oxide Cr_2O_3 was reduced during sintering. A more exhaustive study was therefore undertaken, identifying the parameters that affect the creation of the final microstucture. Several essential aspects of sintering were examined in this study:

- green density,
- oxygen potential of sintering atmosphere,
- doping agent concentration.

The method of incorporating the doping agent is a study parameter in itself. Doping was carried out here by spray-drying. This disperses the additive more homogeneously, owing to the larger grain size obtained by this process in comparison with other methods of inclusion [5,6]. These other mixing processes, such as crushing and stirring together, have been tested elsewhere [5,6] and certain results will be compared with those of the spray-drying process adopted here. Macropores intended to stabilise the density of the sintered metals were introduced to check their effect on grain growth. Changes in microstructure were monitored during annealing operations in order to obtain grain growth kinetics laws.

2. Experimental methods

2.1. Preparation of samples

The powder used for the experiments was obtained by a dry process, involving conversion of gaseous UF_6 into UO_{2+x} by pyrohydrolysis and reduction. The initial O/U ratio was 2.14 and the specific surface area determined by a BET method is about 3.50 $m^2\ g^{-1}$. The size of the elementary crystallites was about 0.2 μm. The total impurities content was less than 160 μg/gU, including 110 μg of carbon.

Cr_2O_3 doping was carried out by spray-drying a suspension containing UO_2 powder in distilled water and a soluble salt, ammonium chromate $(NH_4)_2CrO_4$, as precursor. The spray-drying process did not modify the O/U ratio of the powders nor their specific surface area of 3.50 ± 0.15 $m^2\ g^{-1}$ for the various concentrations obtained. Calcination of the powders in argon completely transformed the chromate into Cr_2O_3 without affecting the O/U ratio of the powders. The UO_2 powder used as test specimen was also sprayed and dried. The prepared powders appeared as spherical particles with a log-normal distribution centred around 30 μm (Fig. 1).

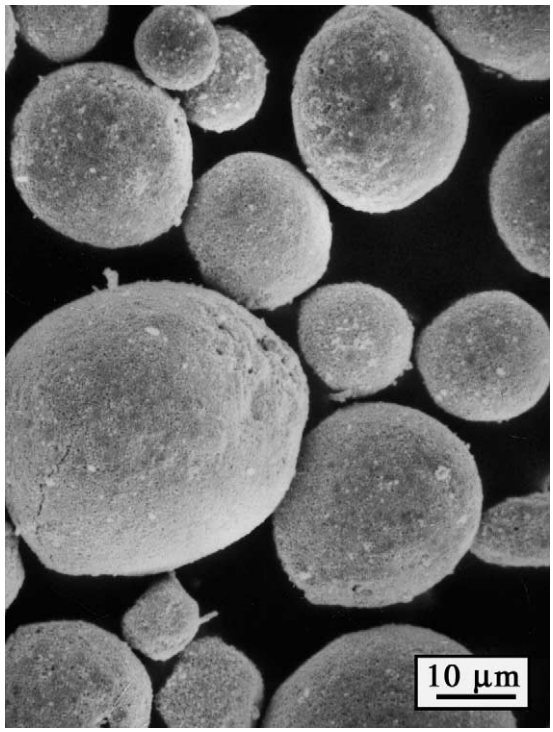

Fig. 1. Spray-dried UO_2 powder doped with Cr_2O_3.

The green pellets are obtained by double-action uniaxial compression of the powder in a die, the walls of which were lubricated with a film of stearic acid previously diluted in ether. A pressure of 300 MPa was sufficient to obtain relative densities of the order of 60%. To adjust the relative density of the sintered samples to about 95%, 1 wt% of a pore former (azodicarbonamide) was added in selected tests after selecting two grain size classes. The pore former was mixed with the sprayed powder for 20 min.

2.2. Sintering

Sintering was performed in hydrogen (5 vpm H_2O and 5 vpm O_2 maximum) with water vapour added using a bath maintained at the temperature adjusted to the required oxygen potential. The quantity of water vapour was controlled by a dew point hygrometer, while the oxygen potential is calculated using the formula proposed by Wheeler and Jones [7].

$$RT\ln(PO_2) = -479070 + 4.184\ T[8.86\log_{10} T - 4.42 + 9.152\log_{10} P(H_2O)/P(H_2)] \quad (J\ mol^{-1}).$$

The relationship between uranium dioxide stoichiometric deviation, temperature and oxygen potential was

derived from the literature survey performed by Lindemer and Besmann [8]. Sample shinkrage was monitored using a vertical differential dilatometer developed in the laboratory, including automatic furnace control and data acquisition. The standard heating cycle involves heating to the sintering temperature at a rate of 150 K h^{-1}, holding for 4 h and then cooling at a rate of 300 K h^{-1}. The temperatures were measured using W5%Re/W26%Re thermocouples placed very close to the pellets. Sintered densities were determined by hydrostatic weighing in ethanol. The theoretical density of the mixtures $\rho_{th}(M)$ was calculated by assuming zero solubility of Cr_2O_3 in UO_2 at room temperature [2], i.e.,

$$\rho_{th}(M) = \%\mathrm{vol}(UO_2)\rho_{th}(UO_2) + \%\mathrm{vol}(Cr_2O_3)\rho_{th}(Cr_2O_3)$$

with $\rho_{th}(UO_2) = 10.96$ g cm^{-3}

and

$\rho_{th}(Cr_2O_3) = 5.21$ g cm^{-3}.

Grain size was determined by the linear intercept method using polished and chemically etched samples. More than 300 intercepts were counted for each sample. Additional observations were made by SEM. Detail identification of the secondary phases using transmission microscopy, electron diffraction and energy-dispersive X-ray spectrometry were also performed on selected sample and are discussed elsewhere [2].

3. Results

3.1. Effect of oxygen potential on grain growth

Fig. 2 shows the oxygen potential levels of the $UO_{2\pm\varepsilon}$ field, Cr/Cr_2O_3 balance [9] and three sintering atmospheres corresponding to ($H_2 + H_2O$) mixtures. In what was considered to be a 'dry' hydrogenous atmosphere ($H_2 + 0.05$ vol.% H_2O), Cr_2O_3 reduction in metallic Cr began at 1000°C whereas when the quantity of water vapour was increased, it is possible to maintain Cr oxidized as Cr_2O_3 throughout the sintering cycle. Variations in grain size as a function of Cr_2O_3 content and the three sintering atmospheres are shown in Fig. 3, following a standard heat treatment cycle. Grain growth of doped UO_2 only appeared to occur within a precise oxygen potential domain. The microstructures of UO_2 containing 0.05 wt% of Cr_2O_3 after sintering in ($H_2 + 0.05$ vol.% H_2O), ($H_2 + 1$ vol.% H_2O) and ($H_2 + 5$ vol.% H_2O) are shown in Figs. 4(a), (b) and (c), respectively.

In a wet sintering atmosphere ($H_2 + 1$ vol.% H_2O), the variations in grain size as a function of Cr_2O_3 and isothermal holding temperature are shown in Fig. 5. The

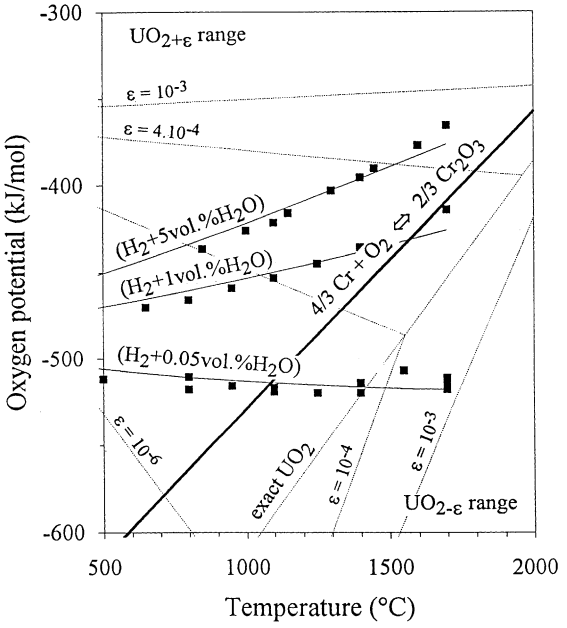

Fig. 2. Ellingham diagram for Cr/Cr_2O_3 according to [9] and for the $UO_{2\pm\varepsilon}$ domain according to [8]. The symbols (■) correspond to oxygen potentials determined from hygrometer recordings. The lines are for smoothed points based on a mean water vapour content kept constant during sintering.

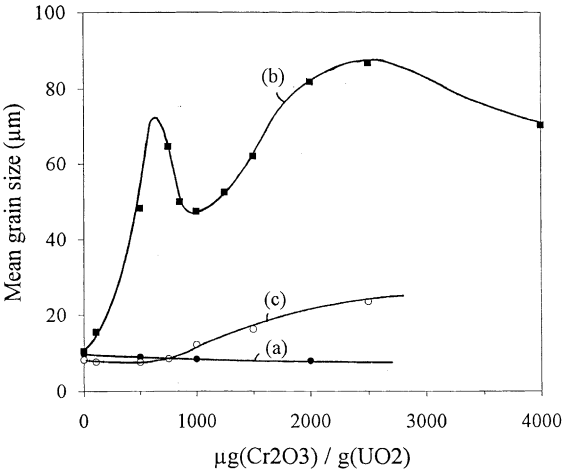

Fig. 3. Relationship between mean grain size and Cr_2O_3 content (after standard heat treatment). (a) $H_2 + 0.05$ vol.% H_2O, (b) $H_2 + 1$ vol.% H_2O and (c) $H_2 + 5$ vol.% H_2O.

relative densities of these samples are listed in Table 1. Above about 1550°C, the curves showing grain size plotted against initial Cr_2O_3 concentration display two peaks, one around 0.07 wt% and the other at about 0.25 wt%.

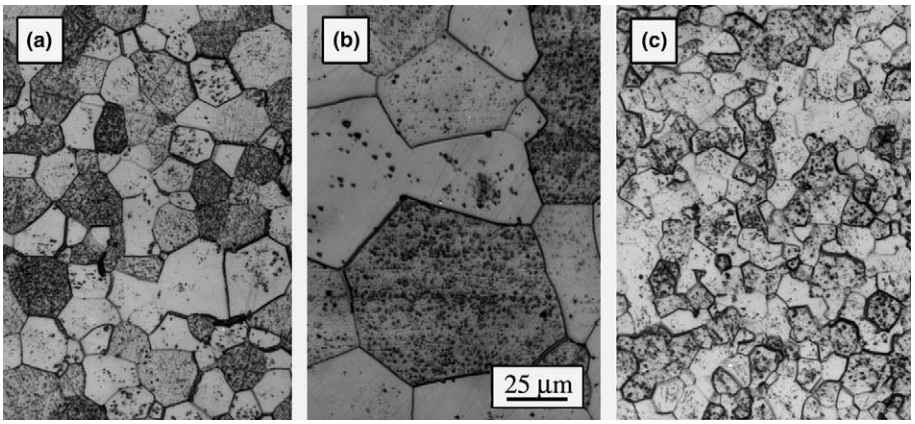

Fig. 4. Optical micrographs of $UO_2 + 0.05$ wt% Cr_2O_3 samples, sintered in: (a) $H_2 + 0.05$ vol.% H_2O, (b) $H_2 + 1$ vol.% H_2O and (c) $H_2 + 5$ vol.% H_2O.

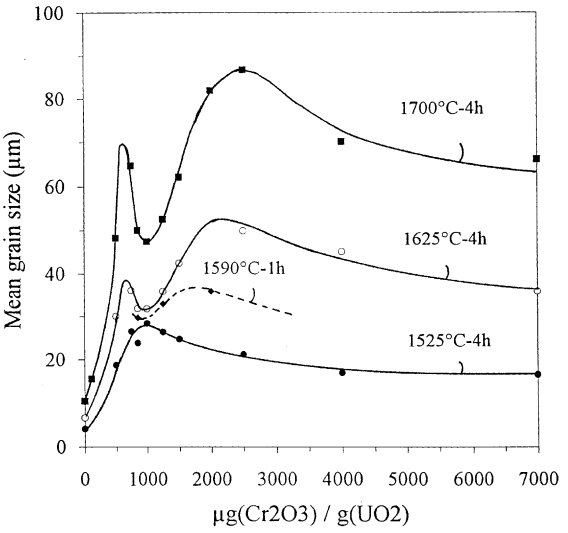

Fig. 5. Relationship between mean grain size and Cr_2O_3 content in $H_2 + 1$ vol.% H_2O (after standard heat treatment).

3.2. Effect of green density on grain growth

The fact that the spray-dried powder is highly compressible means that it is impossible to obtain differences of more than 5–6% in green density by modifying compaction pressure. Dilatometric monitoring of the shrinkage of UO_2 containing 0.1 wt% of Cr_2O_3 compacted at two different pressures (100 and 300 MPa) in ($H_2 + 1$ vol.% H_2O) is shown in Figs. 6(a) and (b) corresponds to the relative shrinkage rates calculated at selected intervals using the relation

$$V(\mathrm{s}^{-1}) = -\frac{h_{i+1} - h_i}{t_{i+1} - t_i}\frac{1}{(h_{i+1} + h_i)/2},$$

where h_i is the height of the sample at time t_i.

Similar experiments were performed with UO_2 containing 0.075 wt% of Cr_2O_3 with a heating rate of 250 K h^{-1}. In these test conditions, a 5–6% difference in green density means that the difference in sintered density is no more than 1% (Table 2). The final grain size and, in theory, the kinetics of grain growth are not affected by this difference (Table 2). In contrast, the intergranular pore volume is directly dependent on the final density reached (the microstructures corresponding to curves 2 and 3 of Fig. 6(a) are shown in Figs. 7(a)–(d)). The grain growth may be considered as abnormal in the sense that the pores does not seem to pin the boundaries.

The doped powders sintered more slowly than the reference powder (Fig. 6). Compaction at 300 MPa provided green densities of the order of 60%. A pore spectrum determined for a green pellet compacted in this way gave a mean pore diameter of 0.2 µm (0.35 µm maximum), which corresponds to the mean size of the crystallites. In spite of this good compression behaviour, the doped samples appeared to memorise the sprayed particle shapes up to density around 90% (Fig. 9). This memory effect seems to be due to segregation of the chromium oxide during the suspension drying phase [5]. Disregarding this segregation, a simple calculation shows that the addition of 0.1 wt% of Cr_2O_3 may be enough to cover about 20% of the surface area developed by the crystallites, i.e., 3.5 $m^2\ g^{-1}$, with a mono-layer of Cr_2O_3. The delay in shrinkage of the spray-doped powder is therefore attributed to the intimate distribution of Cr_2O_3 which hinders the formation of intergranular bridges during the first stage of densification. In contrast, no delay in shrinkage can be seen when Cr_2O_3 is added by mixing or ball-milling the two oxides together [5,6]. It is worth noting Cr_2O_3 solubility in UO_2 is considered to be negligible at these temperatures.

Table 1
Relationship between grain size and Cr_2O_3 additions after standard heat treatment in ($H_2 + 1$ vol.% H_2O)

Cr_2O_3	1525°C – 4 h		1625°C – 4 h		1700°C – 4 h	
(μg/g UO_2)	ρ/ρ_{th} (%)	G (μm)	ρ/ρ_{th} (%)	G (μm)	ρ/ρ_{th} (%)	G (μm)
0	98.23	4.2	–	6.7	99.06	10.5
110	–	–	–	–	99.15	15.5
500	98.94	18.6	–	29.9	99.34	48.2
750	99.24	26.4	–	36.1	99.19	64.7
850	99.15	23.8	–	31.8	99.08	49.9
1000	99.28	28.3	–	31.7	99.33	47.4
1250	99.09	26.3	–	35.8	99.24	52.5
1500	99.22	24.6	–	42.3	99.19	62.1
2000	–	–	–	–	99.22	81.9
2500	99.30	21.1	–	49.8	99.38	86.8
4000	98.93	16.8	–	45.0	98.87	70.2
7000	98.72	15.4	–	35.7	98.79	66.0

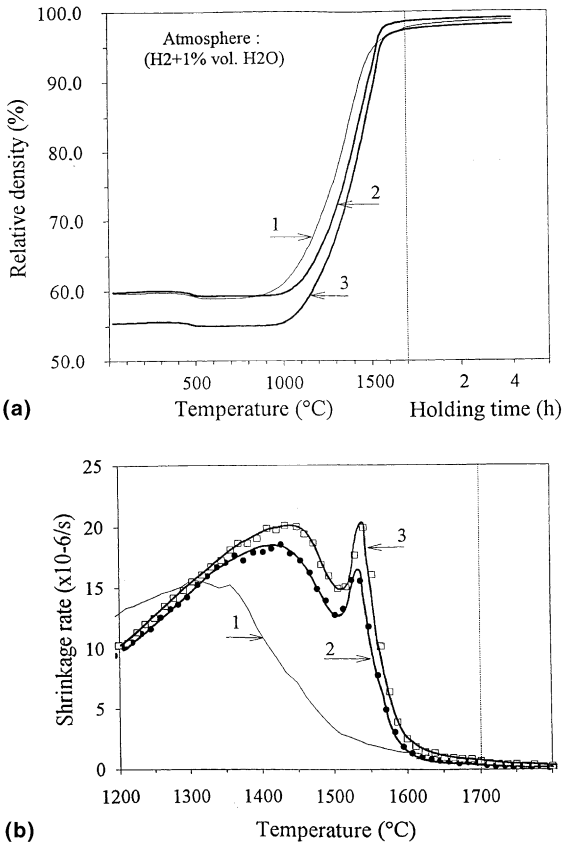

Fig. 6. (a) Shrinkage curves for different UO_2 compacted powder pellets in $H_2 + 1$ vol.% H_2O: (1) undoped UO_2 sample, (2) spray-dried UO_2 powder doped with 0.1 wt% Cr_2O_3, compacted at 300 MPa and (3) same sample, compacted at 100 MPa. (b) Corresponding shrinkage rates vs. temperature.

Fig. 6(b) clearly shows that shrinkage rates accelerate once again above 1500°C in the case of doped samples, which has also been noted with other doping agent distribution methods [5,6]. In the case of the spray-doped samples, the increase in shrinkage rate around 1500°C was demonstrated in ($H_2 + 1$ vol.% H_2O), for all the Cr_2O_3 levels (Figs. 8(a) and (b)), different green densities (Fig. 6(b)) and different rates of temperature increase studied. These features are not observed in the other two sintering atmospheres tested in this study [5].

3.3. Abnormal grain growth stages

3.3.1. Shrinkage and abnormal grain growth

The microstructure changes during the shrinkage acceleration was examined in order to determine the reason for its appearance. For this purpose, the samples were heated at 150 K h^{-1} to the required temperature and held for 1 min. They were then cooled rapidly at 50 K min^{-1} to 1100°C to freeze the microstructure, followed by further cooling at 300 K h^{-1} down to room temperature. The relative densities reached at 1540°C and 1560°C, as well as in isothermal conditions at 1500°C are shown in Table 3. The changes in microstructure at 1500°C is shown in Fig. 9.

Abnormal grains begin to appear around the sides of sprayed UO_2 particles with a still visible memory effect, and then along the crystallisation front until a homogeneous grain structure is obtained. There is thus a close correlation between the appearance of this abnormal grain growth stage and the re-acceleration of shrinkage rates shown in Figs. 6 and 8. However, the continuing grain growth is abnormal in as much that the pores in intergranular positions are left behind by grain boundaries.

3.3.2. Second abnormal growth stage

To determine the behaviour of the microstructure with respect to macropores distribution, a pore former was added to a sprayed UO_2 powder containing 0.2 wt% of Cr_2O_3. Three batches were prepared in this way

Table 2
Influence of green density on grain size after heat treatment in ($H_2 + 1$ vol.% H_2O)

Green density		Sintered density		G (μm)
(g/cm^3)	ρ/ρ_{th} (%)	(g/cm^3)	ρ/ρ_{th} (%)	
$UO_2 + 0.1$ wt% Cr_2O_3 (heating rate: 150 K h^{-1})				
6.07	55.43	10.75_8	98.18	54.2 ± 1.4
6.55	59.79	10.84_9	99.04	52.3 ± 1.5
$UO_2 + 0.075$ wt% Cr_2O_3 (heating rate: 250 K h^{-1})				
6.10	55.69	10.81_0	98.66	59.3 ± 2.4
6.40	58.42	10.85_4	99.06	60.0 ± 2.0
6.64	60.59	10.86_6	99.17	63.2 ± 1.0

(Table 4). Sintering was carried out at slow heating rates (50 K h^{-1}) with a temperature plateau of 1700°C for 1 h in ($H_2 + 1.7$ vol.% H_2O). The pellets then underwent resintering tests at 1720°C in the same atmosphere for 24 h. The densities and grain sizes reached are shown in Table 4. Fig. 10 shows micrographs of batches B and C before the resintering test.

With the same pore former concentration, the pores of the batch B are more numerous thus closer to each other than those of the batch C: 10–20 μm instead of 50–80 μm. Growth in batch B is thus disturbed earlier in the sintering cycle than in C, confirming the sizes of grains obtained prior to annealing. In contrast, during annealing, the grain boundaries of batch B have over-passed most of the macropores while for batch C the macropores are mostly located on the grains boundaries. They seem indeed to exert a much greater disturbing effect on grain boundaries movement, according to the micrographic examinations performed by Buisson et al. [6].

3.4. Study of grain growth kinetics

3.4.1. Impacts of heating rates

The heating rate is often a critical parameter in obtaining specific microstructures. For example, when the densification mechanism has a higher activation energy than that controlling growth, it is preferable to work at high temperatures and fast heating rates in order to obtain very dense small-grained ceramics. This has been observed in the case of fast alumina sintering [10].

Even though the UO_2–Cr_2O_3 system displays two abnormal grain growth stages between 1500°C and 1700°C, sintering was performed at different rates in order to determine whether there was any relation between grain size and heating rate. The tests were performed with three spray-doped powders. Two of these were taken from the batch used so far (doped with 0.075 and 0.2 wt% of Cr_2O_3), while the third (doped with 0.07 wt%) was taken from another dry-process batch with a pre-sintering O/U ratio of 2.08 and a specific surface area almost identical to that of the first batch (3.34 m^2 g^{-1}). The heating cycle adopted in this case was as follows:

- 250 K h^{-1} heating rate up to 1450°C, then followed by rates at rates ranging from 75 to 500 K h^{-1} up to 1700°C
- holding the samples at 1700°C for 1 min,
- rapid cooling at 50 K min^{-1} from 1700°C to 1400°C in order to freeze the microstructure, followed by further cooling at 300 K h^{-1} down to normal temperature.

With the different heating rates applied over this limited temperature range (1450–1700°C), the samples reach identical densification rates (Table 5). In contrast, the heating rate produces considerable variations in grain size: the slower the rate, the larger the grains.

3.4.2. Isothermal conditions

In these tests, all the samples were heated to 1515°C in ($H_2 + 1$ vol.% H_2O) for 15 min in order to achieve the first stage of abnormal grain growth and to obtain homogenous grains of about 20 microns. Isothermal annealing were then carried out at 1515°C and 1700°C. For the 1700°C tests, the annealing temperature is reached as quickly as possible (1000 K h^{-1}). The grain sizes obtained in this way are shown in Table 6, and the corresponding curves in Fig. 11.

The grain size of UO_2 doped with 0.2 wt% of Cr_2O_3 increases from 17 to 51 μm after the temperature had been held at 1700°C for 2 min. It is likely that this considerable grain growth occurs as the temperature rises rather than when it was held steady for 2 min. At 1515°C, the grain size decreased as the Cr_2O_3 content increased from 0.085 to 0.2 wt%, in agreement with the curve obtained at 1525°C (Fig. 5). At 1700°C, on the other hand, the grain size increased when the Cr_2O_3 content increased from 0.085 to 0.2 wt%, still in agreement with the curve obtained at 1700°C (Fig. 5).

4. Discussion

4.1. Shrinkage and abnormal grain growth

Two abnormal growth stages were observed during microstructure development of Cr_2O_3-doped UO_2. The

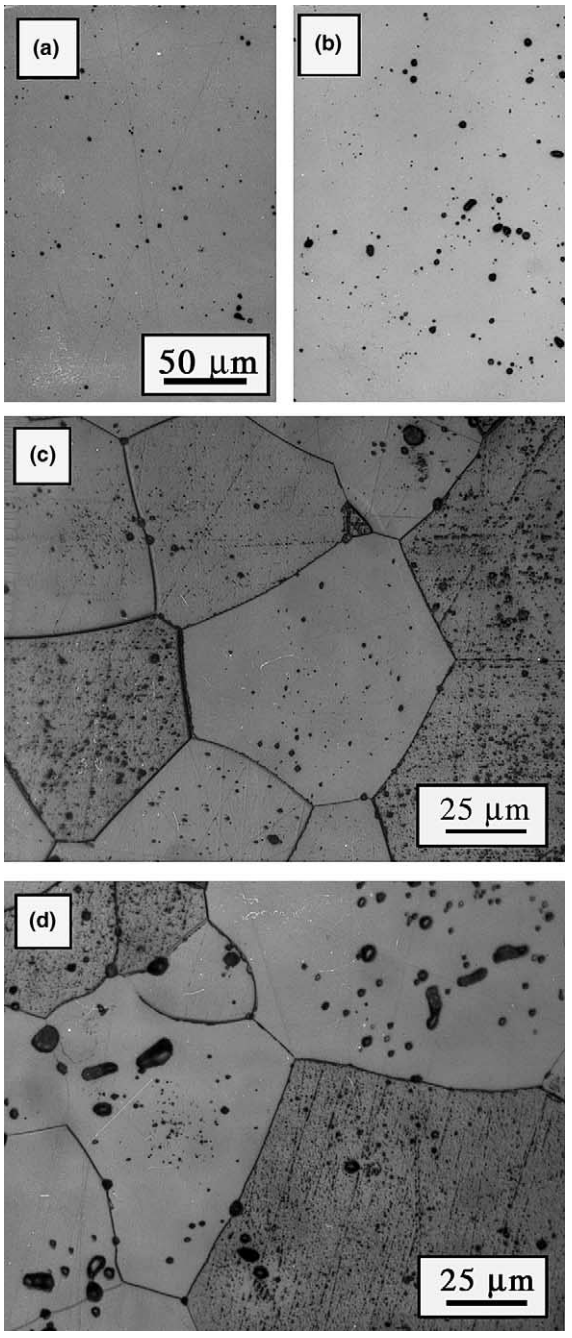

Fig. 7. Optical micrographs before and after chemical etching, corresponding to shrinkage curves nos. 2 ((a) and (c)) and nos. 3 ((b) and (d)) of Fig. 6. Grain growth is hardly affected by residual porosity.

first involves the emergence of an abnormal grain size distribution until the microstructure crystallises, while the second is characterised by boundaries not being pined by residual pores, and even macropores.

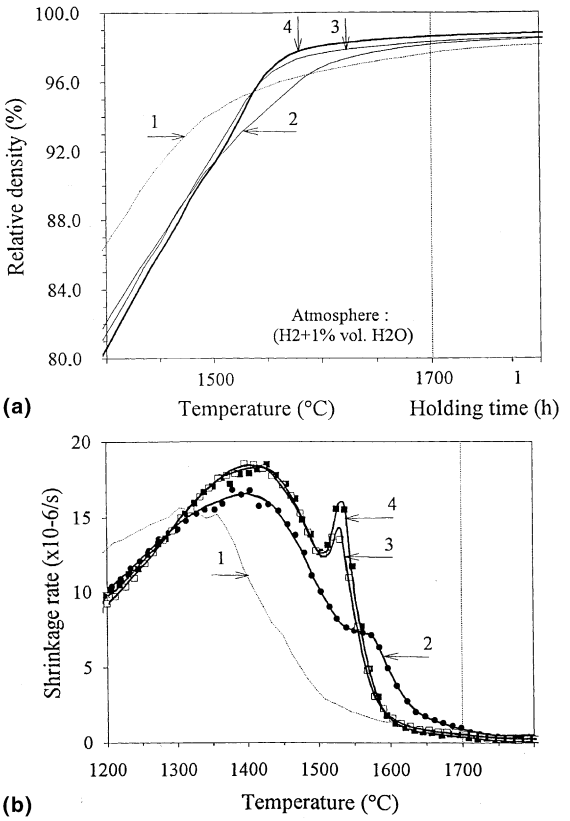

Fig. 8. (a) Shrinkage curves for different UO_2 compacted powder pellets in $H_2 + 1$ vol.% H_2O: (1) undoped UO_2 sample, (2) $UO_2 + 0.05$ wt% Cr_2O_3, (3) $UO_2 + 0.075$ wt% Cr_2O_3 and (4) $UO_2 + 0.1$ wt% Cr_2O_3. (b) Corresponding shrinkage rates vs. temperature, showing the net increase at relative densities of about 93% of theoretical density.

4.1.1. First stage

Generally, abnormal grain growth takes place to the detriment of shrinkage as grain boundaries pass of the pores. With Cr_2O_3, abnormal growth occurs simultaneously (Fig. 9) with an acceleration in densification above 1500°C (Figs. 6 and 8). Fig. 12 shows the crystallisation front eliminating the residual pores within the matrix grains.

A similar phenomenon was reported by Xue and Brook [11,12]. They interpreted the accelerated elimination of porosity in the presence of abnormal grains as being due to the appearance of curvatures favourable to the elimination of matrix pores when they are intersected by an abnormal grain boundary. In the example described by the authors, the abnormal grains of $BaTiO_3$ were also dense, but the abnormal grain growth stage occurred in a non-doped ceramic. In our work, this stage occurred in a two-phased ceramic for most of the sintering cycle (Fig. 9(a)). Late dissolution of the Cr_2O_3 affects both the initiation of abnormal growth and the

Table 3
Variation in relative density ρ/ρ_{th} (%) with heat treatment, in the region of increase in densification rate (see dilatometric curves for more details)

Heat treatment	Cr_2O_3 (wt%) None	Cr_2O_3 (wt%) 0.075	Cr_2O_3 (wt%) 0.25
1500°C – 1 min	96.81	93.98	93.81
1500°C – 6 min	97.33	96.23	95.84
1500°C – 16 min	97.45	96.67	97.36
1540°C – 1 min	97.22	97.25	97.74
1560°C – 1 min	97.68	98.41	98.39

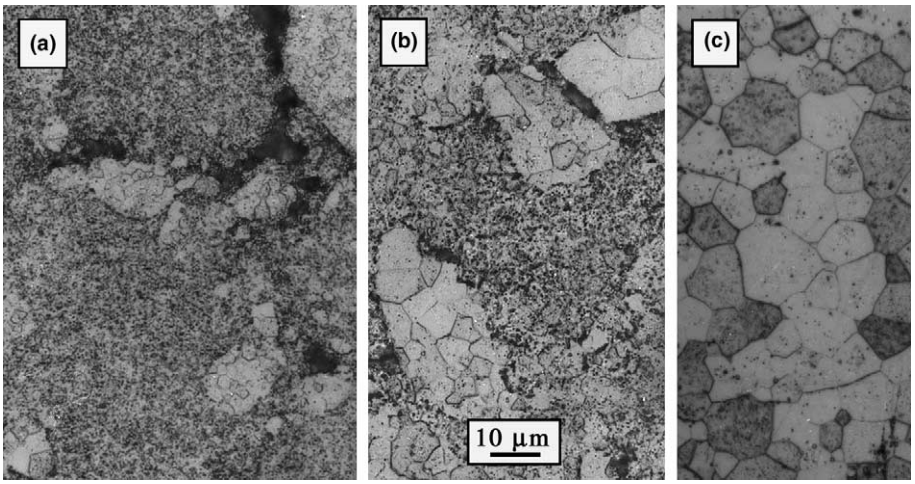

Fig. 9. Microstructural change in the densification acceleration zone of $UO_2 + 0.2$ wt% Cr_2O_3 held at 1500°C for 1 min (a), 6 min (b) and 16 min (c). The abnormal grain growth occurring here has a rapid and considerable effect on grain size and relative density.

Table 4
Correlation between pore former size and final grain size of UO_2 doped with 0.2 wt% Cr_2O_3

	Batch A	Batch B	Batch C
Characteristics of pore former	–	0.9 wt% added	0.9 wt% added
	–	$10 < \Phi < 35$ µm	$40 < \Phi < 63$ µm
Green density (g/cm^3)	6.56 ± 0.01	6.42 ± 0.01	6.42 ± 0.01
Sintered density (g/cm^3)	10.84 ± 0.01	10.42 ± 0.01	10.41 ± 0.01
ρ/ρ_{th}(%)	98.9 ± 0.1%	95.0 ± 0.1%	95.0 ± 0.1%
Grain size (µm)	156	80	110
Resintering test: 1720°C – 24 h in (H_2 + 1.7 vol.% H_2O)			
Densification (%)	−0.1	−0.3	−0.1
Grain size (µm)	175	130	140

kinetics of densification. The action of a eutectic liquid between Cr and Cr_2O_3 is rejected for this first stage because abnormal grain growth took place at a temperature that is too low for the eutectic change to occur.

4.1.2. Second stage

After the first stage of abnormal growth, a population of homogeneous grains quickly appears. However, continuing growth between 1550°C and 1700°C is once again accompanied by an abnormal growth stage as the pores are located into intragranular positions. This microstructure development deserves further investigation with the aim to describe the interactions between the grains and the pores more precisely. However, examination of the pores in Fig. 7(d), where sizes of several µm can be observed, suggests simultaneous growth of both

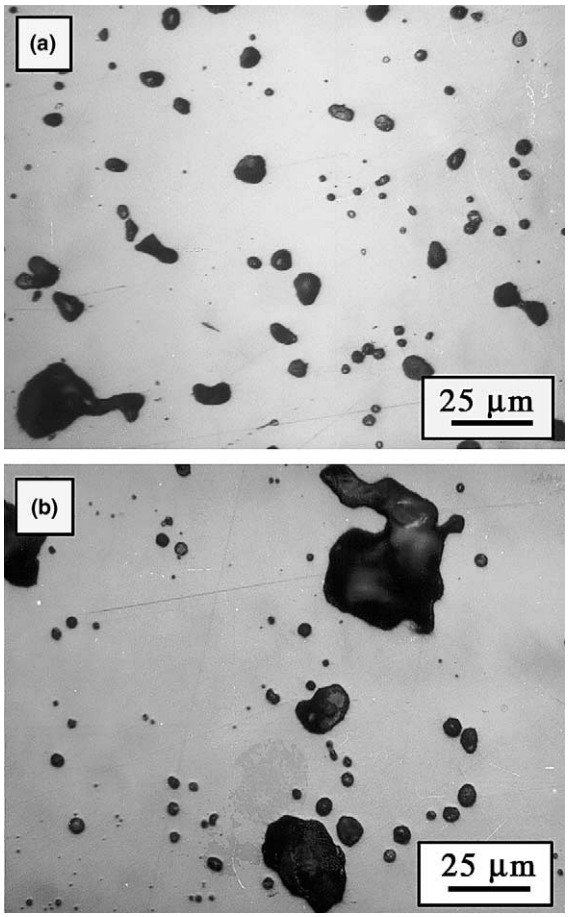

Fig. 10. Unetched optical micrographs of batches B and C (see Table 4) before resintering test, showing pore size obtained from two classes of pore former.

grains and pores. It can be shown that, in the presence of macropores, the more finely divided the pore former, the more grain growth slows down (Table 4). This effect is less obvious during annealing, as the mobility of the grain boundaries in the UO_2–Cr_2O_3 system enables them to pass off pores of up to 20 μm diameter, which is no longer the case with the 40–63 μm pores of batch C.

4.2. Limits of Cr_2O_3 solubility in UO_2

According to the results given in Table 2, residual pore volume has very little effect on final grain size for the difference in green density obtained. This aspect has already been highlighted in another paper [2]. Consequently, the curves showing grain size variation against Cr_2O_3 concentration (Fig. 5) can be interpreted as follows:

- as long as the doping agent is dissolved at a given temperature, grain growth occurs easily,
- beyond the solubility limit, excess doping agent remains as inclusions that pin the grain boundaries (cf. Fig. 5 for temperatures below 1550°C).

When a microstructure contains precipitates, the grains reach a maximum size $\overline{G_m}$, fixed by a relation proposed by Zener [13] linking precipitate size and volume fraction with $\overline{G_m}$. From this analysis, it was possible to propose a solubility limit at 1700°C at about 0.07 wt% of Cr_2O_3 in UO_2 [2]. This approximate solubility limit was confirmed by transmission electron microscopy examination of the precipitates, the size of which was found to be of the order of several tens of nanometers with initial concentrations of less than 0.075 wt%, thus confirming their nucleation on cooling of the solid solution [2]. The other curves in Fig. 5 confirm this value of 0.07 wt% for all the temperature range studied 1500–1700°C.

The grain sizes shown in Fig. 5 are characteristic of a precise heat treatment cycle, in particular the heating rate chosen, and cannot be considered as maximum grain sizes, $\overline{G_m}$. The heating cycle determines, for example, the size of the grain population, which increases

Table 5
Influence of heating rate on grain size of Cr_2O_3-doped fuel

Heating rate (K h^{-1})	Grain size		
	Relative density, ρ/ρ_{th} (%)		
	Cr_2O_3 (wt%) 0.07	Cr_2O_3 (wt%) 0.075	Cr_2O_3 (wt%) 0.2
75	49.6 $\mu m^{+0.7}_{-1.2}$	45.9 $\mu m^{+1.2}_{-1.5}$	73.2 $\mu m^{+0.6}_{-0.7}$
	99.39	99.27	99.27
100	–	–	68.4 $\mu m^{+0.8}_{-1.1}$
	–	–	–
150	35.4 $\mu m^{+1.2}_{-1.0}$	32.2 $\mu m^{+1.2}_{-1.8}$	63.4 $\mu m^{+0.7}_{-0.8}$
	99.45	99.39	99.41
300	21.5 $\mu m^{+0.3}_{-0.5}$	19.5 $\mu m^{+0.5}_{-0.4}$	38.0 $\mu m^{+0.5}_{-0.6}$
	99.30	98.92	98.97
500	18.3 $\mu m^{+0.5}_{-0.8}$	15.3 $\mu m^{+0.5}_{-0.7}$	32.8 $\mu m^{+0.3}_{-0.3}$
	99.35	99.05	99.19

Table 6
Grain sizes achieved after different annealing times at 1515°C and 1700°C in ($H_2 + 1$ vol.% H_2O)

Cr_2O_3 added (wt%)	Annealing time (min)	Annealing temperature	
		1515°C	1700°C
		Grain size (μm)	Grain size (μm)
0	0	4.0 ± 1.0	–
	2	–	6.5 ± 0.6
	60	–	10.7 ± 0.9
	360	–	18.6 ± 1.2
	720	9.4 ± 0.4	22.2 ± 1.7
0.085	0	22.3 ± 1.0	–
	2	–	32.5 ± 1.9
	60	27.6 ± 1.3	38.9 ± 2.5
	150	32.2 ± 1.3	45.2 ± 3.4
	360	37.0 ± 2.3	51.1 ± 4.3
	720	–	51.8 ± 2.3
0.125	0	19.7 ± 1.0	–
	2	–	35.6 ± 1.9
	60	25.3 ± 1.1	46.9 ± 3.6
	150	29.6 ± 1.5	58.6 ± 5.6
	360	34.7 ± 2.0	62.4 ± 6.0
	720	35.5 ± 2.1	63.8 ± 3.4
0.2	0	17.0 ± 0.5	–
	2	–	50.8 ± 2.0
	60	23.3 ± 0.9	58.0 ± 4.0
	150	26.3 ± 1.2	64.2 ± 3.5
	360	29.2 ± 1.5	70.3 ± 2.2
	720	32.9 ± 1.8	73.0 ± 4.0

through Ostwald ripening, according to research carried out by Peres et al. [14,15]. The secondary phase also undergoes a change in composition in ($H_2 + 1$ vol.% H_2O), which depends on the high temperature holding time (cf. 4.3 and 4.4). However, the interpretation of the curves from Fig. 5 to determine a solubility limit is not modified: when annealing is prolonged, the grain size increases, but always as shown in Fig. 5 (cf. 4.4).

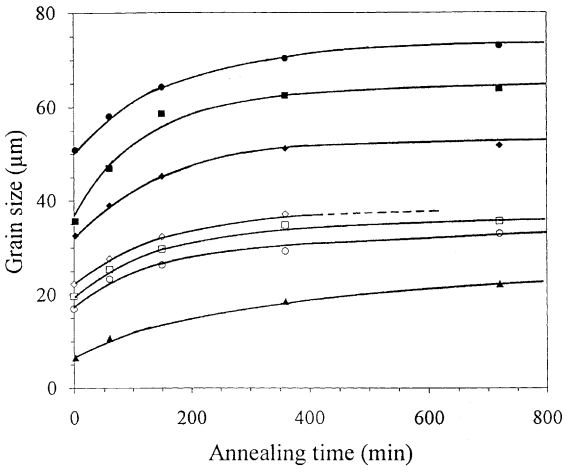

Fig. 11. Grain size as a function of time and temperature. (▲) pure UO_2 at $T = 1700$°C; (○, ●) $UO_2 + 0.2$ wt% Cr_2O_3 at $T = 1515$°C and 1700°C; (□, ■) $UO_2 + 0.125$ wt% Cr_2O_3 at $T = 1515$°C and 1700°C; and (◇, ◆) $UO_2 + 0.085$ wt% Cr_2O_3 at $T = 1515$°C and 1700°C.

4.3. Existence of a eutectic in the Cr–Cr_2O_3 system

In ($H_2 + 1$ vol.% H_2O), above 1550°C, a second grain growth activation mechanism occurs beyond 0.1 wt% of Cr_2O_3, i.e., beyond the proposed solubility limit (Fig. 5).

Ol'shanskii and Shlepov [16] studied Cr–Cr_2O_3 mixtures in purified argon. According to their analysis of quenched samples, these mixtures appear to be in equilibrium up to a temperature of 1660°C, corresponding to a eutectic with a composition close to CrO. Healy and Schottmiller [17] studied part of the Cr–Si–O ternary system in reducing atmospheres at controlled oxygen partial pressures. The CrO composition was also considered by these authors and the presence of silica would provide mixtures that melt at 1400°C with 41 mol% of SiO_2 and 59 mol% of CrO. Toker et al. [18] recently presented a thermodynamic study of the Cr–O system between 1500°C and 1825°C. Fig. 13 plots the domains

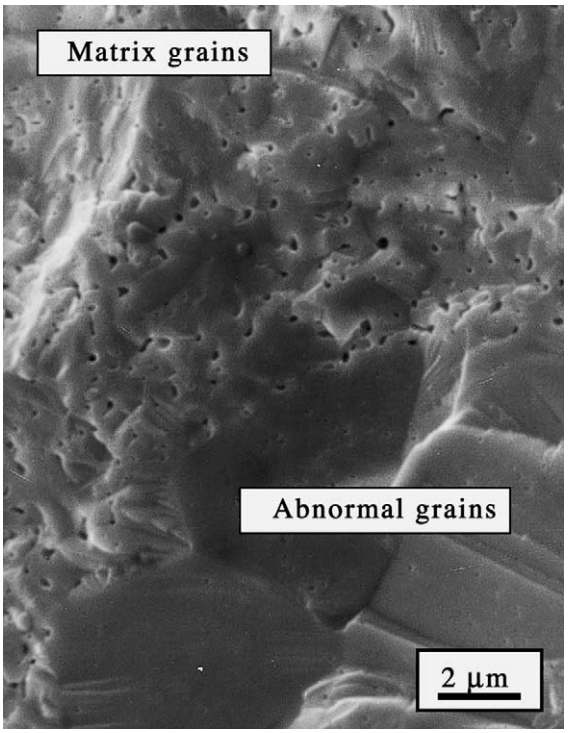

Fig. 12. SEM fracture surface of UO_2 doped with 0.25 wt% Cr_2O_3, showing the development of dense abnormal grains inside a fine-grain matrix.

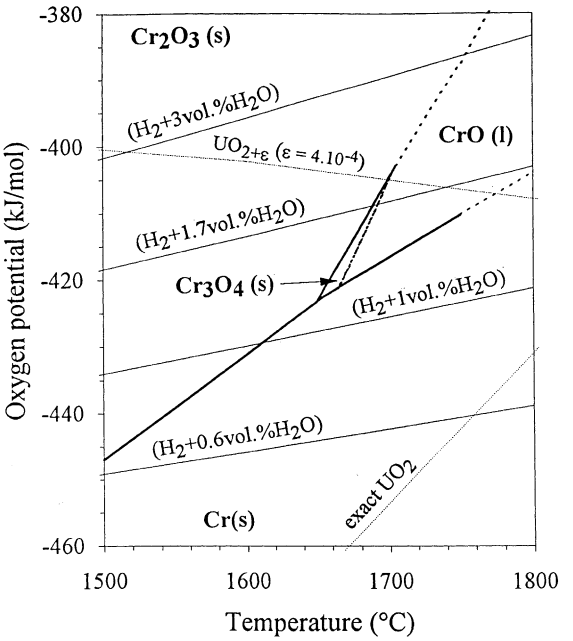

Fig. 13. Thermodynamic equilibrium between metallic Cr and Cr oxides, according to [18]. The stability domain of the CrO composition is also indicated (cf. [18]). The oxygen potentials of four (H_2/H_2O) mixtures are shown.

in which CrO and Cr_3O_4 exist, as determined by Toker et al. [18] together with the oxygen potentials of a few reducing atmospheres. A eutectic can thus be formed in the temperature and oxygen potential ranges that we have explored in the present work to activate grain growth. The existence of this eutectic is confirmed by the following points:

- The grain boundary shapes and Cr_2O_3 content.

At 1525°C, irrespective of the initial Cr_2O_3 content, the grains are equiaxial and show no sign of rounding. At 1700°C, there is a distinct difference in grain morphology depending on the activation mechanism involved: the 0.1 wt% Cr_2O_3-doped sample continues to have equiaxial grains whereas the 0.25 wt% UO_2-doped grains show distinctly rounded edges (Fig. 14).

- Precipitate morphology.

Above the proposed solubility limit for Cr_2O_3 in UO_2 at 1700°C, precipitation became detectable using an optical microscope and its morphology suggests the formation of a liquid phase, according to its 'pool-like' appearance (Fig. 15). This liquid phase cannot be attributed simply to the chromium, since it has a melting point of 1857°C, according to recent calculations by Chase [19]. Energy-dispersive X-ray analyses carried out on the two phases with the same electron acceleration voltage revealed two oxygen concentrations that correspond to the contrast in the precipitates seen under an optical microscope [5]. The white precipitates in Fig. 15 can thus be attributed to metallic Cr and the grey to Cr_2O_3.

With regard to the grain growth reactivation mechanisms, it is therefore assumed that dissolution and precipitation of the uranium oxide take place through the liquid secondary phase.

4.4. Study of grain growth kinetics

4.4.1. Non-isothermal conditions

Grain growth kinetics in porous systems can be formulated as follows:

$$\overline{G}^n(\mathrm{t}) - \overline{G_\mathrm{o}}^n = \frac{k_\mathrm{o}}{T}\exp\left(\frac{-Q}{RT}\right)t, \tag{1}$$

where $\overline{G_\mathrm{o}}$ is the grain size at $t = t_\mathrm{o}$ and n depends on the mechanism controlling grain boundary migration. k_o is a constant and Q is the growth mechanism activation energy. In non-isothermal conditions, Eq. (1) thus becomes

$$\overline{G}^n(t,T) = \overline{G_\mathrm{o}}^n + k_\mathrm{o}\int_{t_\mathrm{o}}^{t}\frac{\exp(-Q/RT)}{T}\,\mathrm{d}t. \tag{2}$$

In experiments with constant heating rates defined by $v = \mathrm{d}T/\mathrm{d}t = \mathrm{etc}$, relation (2) becomes

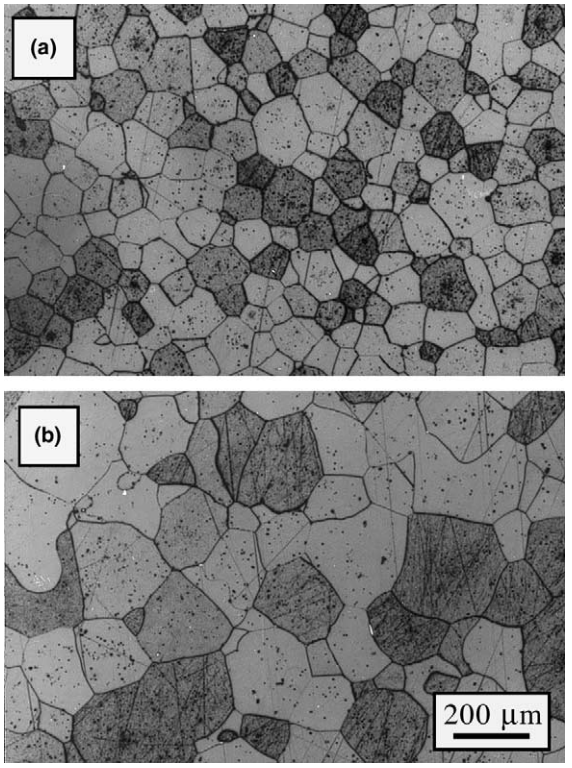

Fig. 14. Optical micrographs of (a) $UO_2 + 0.1$ wt% Cr_2O_3 and (b) $UO_2 + 0.25$ wt% Cr_2O_3 (after standard heat treatment in $H_2 + 1$ vol.% H_2O). Note the flattening of the grains with high Cr_2O_3 content.

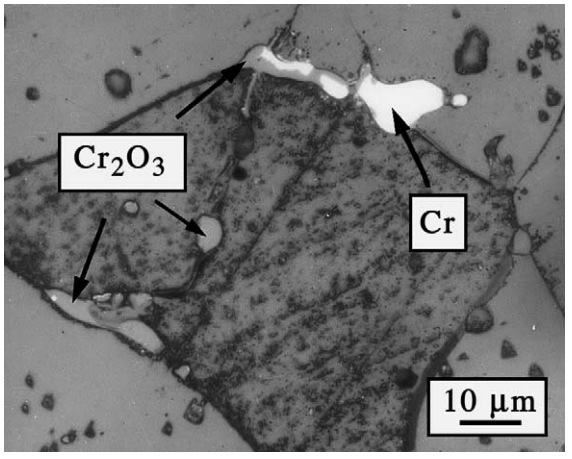

Fig. 15. Morphology of the secondary phase of a sample of UO_2 initially containing 0.25 wt% Cr_2O_3 (with standard heat treatment at 1700°C in $H_2 + 1$ vol.% H_2O). The secondary phase consisting of metallic Cr and Cr_2O_3 [5] is assumed to have been liquid on the basis of its morphology.

$$\overline{G}^n(T) = \overline{G_o}^n + \frac{k_o}{v}\int_{T_o}^{T}\frac{\exp(-Q/RT)}{T}\,dT. \tag{3}$$

With the grain sizes used in the experiments, it was not possible to obtain a linear relation between $\overline{G}^n$ and the reciprocal of the heating rate $1/v$ for the entire range of heating rates explored. Fig. 16 shows, for example, $\overline{G}^3$ plotted as a function of $1/v$. For the three additions of Cr_2O_3 studied here, two kinetic regimes occur: one for heating rates below 200 K h^{-1}, and the other for rates above 200 K h^{-1}.

The existence of the first stage of abnormal growth is enough in itself to prevent relation (3) from being perfectly observed. Irrespective of heating rate, the system with 0.2 wt% of Cr_2O_3 displays larger grain sizes than the systems containing 0.07 and 0.075 wt% of Cr_2O_3, confirming the effect of the insoluble fraction on grain growth. However, it is still difficult to interpret the two kinetic regimes. In light of the results described earlier, the change in composition of the secondary phase in ($H_2 + 1$ vol.% H_2O) is probably different depending on the heating rate chosen. With high rates, there is perhaps less liquid phase than Cr_2O_3 inclusions. In contrast, at low heating rates, a greater fraction of Cr_2O_3 can be reduced, thus enhancing the occurrence of the liquid phase, which activates a fast grain growth kinetics.

4.4.2. Isothermal conditions

The quantity of Cr_2O_3 in the samples used in the experiments is above the proposed solubility limit. Apart from the curve for undoped UO_2, the results shown in Fig. 11 could not be described by classical power laws; these call for exponents higher than $n = 6$, which, according to Brook [20], have no physical meaning. Another formulation proposed by Burke [21] and initially tested by Ainscough et al. [22] on UO_2 was chosen to take into account precipitate pining forces. In the simplest cases, assuming the pining force to be independent of the mean grain size:

$$\frac{d\overline{G}}{dt} = \frac{a}{\overline{G}} - b \tag{4}$$

$$\text{with } \frac{d\overline{G}}{dt} \to 0 \text{ when } \overline{G} = \overline{G_m} \to \frac{a}{b}.$$

The term $a/\overline{G}$ is drawn from Burke and Turnbull analysis [23], which gives an exponent $n = 2$. Another kinetic equation is obtained by integrating (4):

$$\overline{G_m}^2 \ln\left(\frac{\overline{G_m} - \overline{G_o}}{\overline{G_m} - \overline{G}(t)}\right) - \overline{G_m}(\overline{G}(t) - \overline{G_o}) = \frac{k_o}{T}\exp(-Q/RT)t \tag{5}$$

or more simply

$$f(\overline{G_m}, \overline{G_o}, \overline{G}(t)) = k(T)t.$$

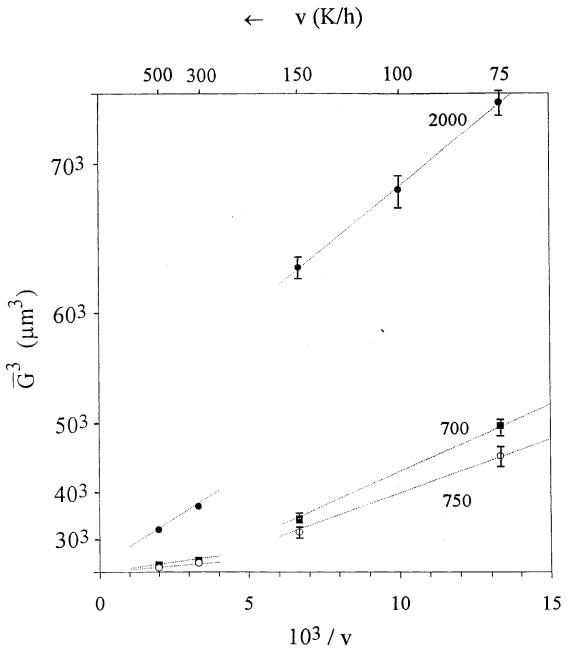

Fig. 16. Plot of $\overline{G}^3$ (final grain size) vs. reciprocal of various heating rates, v^{-1}, for three Cr_2O_3 contents, 700, 750 and 2000 μg Cr_2O_3/gUO_2.

The $\overline{G_m}$ sizes are adjusted to obtain the highest possible correlation coefficient. Figs. 17 and 18 show that relation (5) is suitable for describing the changes in grain kinetics, for contents above the Cr_2O_3 solubility limit in UO_2.

At 1515°C, grain size is limited mainly by the number of Cr_2O_3 precipitates, in agreement with Fig. 13 and

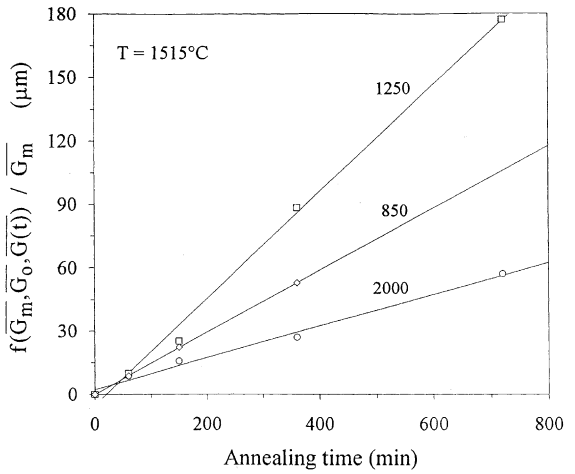

Fig. 17. Plots of $f(\overline{G_m},\overline{G_o},\overline{G}(t))/\overline{G_m}$ as a function of time at $T = 1515$°C, as defined by (5). Legend as for Fig. 11. Good fits of experimental data support the existence of limiting grain sizes for doped samples.

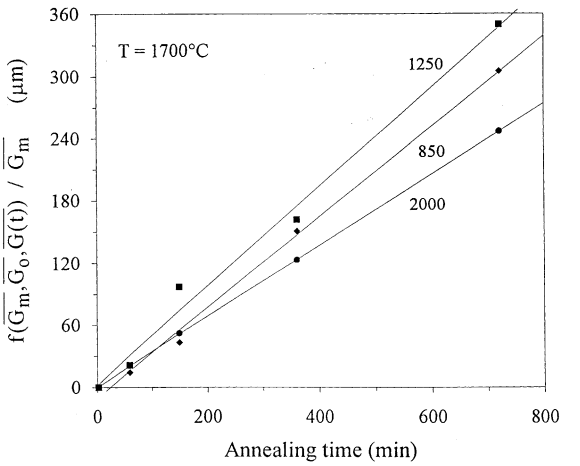

Fig. 18. Plots of $f(\overline{G_m},\overline{G_o},\overline{G}(t))/\overline{G_m}$ as a function of time at $T = 1700$°C, as defined by (5). Legend as for Fig. 11. Good fits of experimental data support the existence of limiting grain sizes for doped samples.

according to the examination of the precipitates by optical microscope. At 1700°C, the occurrence of a liquid phase allows the system containing the highest Cr_2O_3 content to reach larger grain sizes. The effect of the liquid phase, of composition corresponding to CrO, on grain growth is definitely transient owing to the narrow stability domain of this phase in (H_2 + 1 vol.% H_2O) at 1700°C. A large fraction of metallic chromium must develop during annealing and interact with the grain boundaries, thus explaining the maximum grain sizes also observed at 1700°C.

5. Conclusions

A study of variations in grain size as a function of Cr_2O_3 concentration has revealed a solubility limit for this doping agent in stoichiometric UO_2, namely around 0.07 wt% in the 1500–1700°C temperature range. The observed precipitation is in agreement with the oxygen potentials of the sintering atmospheres. Furthermore, the existence of a eutectic between Cr and Cr_2O_3 seems to be confirmed by examining the morphologies of the UO_2 grains and precipitates and studying grain growth in these systems. This liquid phase, the effects of which begin to appear at 1550°C, activates grain growth in samples with a Cr_2O_3 content higher than the proposed solubility limit. The microstructural features of the UO_2–Cr_2O_3 system have a significant impact on densification and grain growth of Cr_2O_3-doped UO_2.

An abnormal grain growth stage promoting densification was also revealed by dilatometric analysis and microstructural examinations. A second stage of abnormal growth then occurs through offsetting of the

residual sintering pores, or even macropores produced by pore formers. In these conditions, the effect of residual pore volume on final grain size is of secondary importance in comparison with the role played by precipitation. Adding pore formers slows down grain growth. However, pores up to 20 μm in size may be displaced during resintering tests, leading to a new type of microstructure compared with those currently used in PWR type reactors. The study of grain growth kinetics showed that they could be represented by laws involving a maximum grain size determined by the characteristics of the precipitation.

Acknowledgements

This work was made possible thanks to financial support from Framatome. The authors wish to thank Professor J.F. Baumard of the *Ecole Nationale Supérieure de Céramiques Industrielles* in Limoges for his scientific contribution to the thesis work of L. Bourgeois. This work has been carried out at the Fuel Radiometallurgy Laboratory of the Department of Thermal Hydraulics and Physics.

References

[1] L. Bourgeois, Ph. Dehaudt, C. Lemaignan, J.P. Frederic, J. Nucl. Mater. 295 (2001) 73.
[2] L. Bourgeois, V. Peres, Ph. Dehaudt, J. Nucl. Mater (to be submitted).
[3] J.B. Ainscough, L.F.A. Raven, P.T. Sawbridge, Int. Symp. on Water reactor fuel fabrication with special emphasis on its effect on fuel performance, Prague, Nov. 6–10 (1978) IAEA-SM233.
[4] J.C. Killeen, J. Nucl. Mater. 88 (1980) 177.
[5] L. Bourgeois, PhD thesis, INPG Grenoble (France) 1992.
[6] P. Buisson, P. Dehaudt, M. Bailleux, M. Guibert, private communication.
[7] V.J. Wheeler, I.G. Jones, J. Nucl. Mater. 42 (1972) 117.
[8] T.B. Lindemer, T.M. Besmann, J. Nucl. Mater. 130 (1985) 473.
[9] JANAF, Thermochemical Tables, 2nd Ed., 1985.
[10] M.P. Harmer, E.W. Roberts, R.J. Brook, Trans. Brit. Ceram. Soc. 78 (1979) 22.
[11] L.A. Xue, R.J. Brook, J. Am. Ceram. Soc. 72 (1989) 341.
[12] L.A. Xue, J. Am. Ceram. Soc. 72 (1989) 536.
[13] C. Zener, quoted by C.S. Smith, Trans. AIME 175 (1949) 15.
[14] V. Peres, PhD thesis, INPG Grenoble (France) 1993.
[15] V. Peres, P. Dehaudt, Proceedings of the International Conference on Materials and Advanced Processes, Euromat 93, Paris, 1993.
[16] Y.I. Ol'Shanskii, V.K. Shlepov, Dokl. Akad. Nauk. S.S.S.R. 91 (1953) 563.
[17] G.W. Healy, J.C. Schottmiller, Trans. Metall. Soc. AIME 230 (1964) 421.
[18] N.Y. Toker, L.S. Darken, A. Muan, Metall. Trans. B 22 (1991) 225.
[19] M.W. Chase, Bull. Alloy Phase Diagrams 4 (1983) 124.
[20] R.J. Brook, in: F.F.Y. Waying, Treatise Material Science Technology, vol. 9-Ceramics, Academic Press, New York 1979, p. 331.
[21] J.E. Burke, Trans. AIME 180 (1949) 73.
[22] J.B. Ainscough, B.W. Oldfield, J.O. Ware, J. Nucl. Mater. 49 (1973/74) 117.
[23] J.E. Burke, D. Turnbull, Progr. Met. Phys. 3 (1952) 220.